Review Article

Elucidation of Sulfoserine Fragmentation Routes and Structures of Key Product Ions

Mrs. Aparna M. Lad, Dr. Baljeet Singh Khurana

Department of Pharmacy, Sabarmati University, Ahmedabad, Gujarat, India

Received: 11-03-2024 / Revised: 19-04-2024 / Accepted: 27-05-2024
Corresponding author: Mrs. Aparna M. Lad
Conflict of interest: Nil

Abstract

Post-translational modifications play a crucial role in regulating protein structure, function, and cellular signaling pathways. Among these modifications, sulfation is an important biochemical process that influences protein–protein interactions and biological activity. The present study aimed to investigate the fragmentation pathways of protonated sulfoserine and to elucidate the structures of the major product ions formed following modification loss. Collision-induced dissociation (CID) experiments revealed two dominant fragmentation channels corresponding to the loss of SO_3 and H_2SO_4, producing fragment ions at m/z 106 and m/z 88, respectively. Infrared multiple photon dissociation (IRMPD) spectroscopy, combined with density functional theory (DFT) calculations at the B3LYP/aug-cc-pVTZ level, was employed to characterize the structures of these fragment ions. The m/z 106 product ion was confirmed to be structurally identical to protonated serine through direct comparison with experimental and theoretical spectra. Structural analysis of the m/z 88 ion demonstrated that it adopts a 2-carboxy-aziridine structure formed via a kinetically controlled fragmentation pathway. The experimental findings showed excellent agreement with theoretical predictions, highlighting the utility of combining ion spectroscopy and computational chemistry for structural elucidation. Furthermore, inter-laboratory comparisons demonstrated the reproducibility and reliability of IRMPD measurements across different instrumental platforms. This work provides detailed mechanistic insight into sulfoserine fragmentation and contributes to a broader understanding of the gas-phase behavior of sulfated biomolecules, facilitating improved interpretation of tandem mass spectrometric data in proteomic studies.

Keywords: Sulfoserine, Fragmentation pathways, Collision-induced dissociation, Infrared multiple photon dissociation, Density functional theory

This is an Open Access article that uses a fund-ing model which does not charge readers or their institutions for access and distributed under the te rms of the Creative Commons Attribution License (http://creativecommons.org/licenses/by/4.0) and the Budapest Open Access Initiative (http://w ww.budapestopenaccessinitiative.org/read), which permit unrestricted use, distribution, and reproduction in any medium, provided original work is properly credited.

Introduction

Post-translational modifications (PTMs) are essential biochemical processes that expand the structural and functional diversity of proteins beyond the information encoded by the genome. Among the various PTMs, sulfation is a widespread modification that plays a significant role in numerous biological functions, including cell signaling, molecular recognition, immune responses, and protein–protein interactions. Sulfated amino acids and peptides are frequently encountered in biological systems, where sulfation contributes to the regulation of protein activity and stability. Consequently, understanding the gas-

phase behavior and fragmentation characteristics of sulfated biomolecules is of considerable importance for analytical and structural biology.

Mass spectrometry has emerged as one of the most powerful tools for the identification and characterization of post-translationally modified proteins and peptides. Tandem mass spectrometry (MS/MS), particularly collision-induced dissociation (CID), provides valuable information regarding molecular structure and fragmentation mechanisms. However, sulfated compounds often exhibit complex fragmentation behavior due to the labile nature of the sulfate group, which can undergo neutral loss during activation. Such fragmentation pathways can complicate spectral interpretation and hinder the accurate identification of sulfation sites.

Sulfoserine serves as an important model compound for investigating the dissociation behavior of sulfated amino acids. Previous studies have demonstrated that CID of protonated sulfoserine predominantly results in the loss of sulfur trioxide (SO_3) and sulfuric acid (H_2SO_4), generating characteristic fragment ions. Although these fragmentation channels are readily observed, the precise structures and mechanisms associated with the resulting product ions have remained subjects of scientific interest.

Infrared multiple photon dissociation (IRMPD) spectroscopy has emerged as a powerful analytical technique for the structural characterization of gas-phase ions. By providing vibrational spectra that can be directly compared with theoretical predictions, IRMPD enables unambiguous identification of ion structures that cannot be distinguished by mass spectrometry alone. When combined with density functional theory (DFT) calculations, IRMPD spectroscopy offers a comprehensive approach for elucidating fragmentation pathways and determining product ion geometries.

In the present study, CID, IRMPD spectroscopy, and theoretical calculations were employed to investigate the fragmentation behavior of protonated sulfoserine. Particular emphasis was placed on identifying the structures of the major fragment ions produced by SO_3 and H_2SO_4 loss. The study provides detailed mechanistic insight into sulfoserine dissociation and demonstrates the effectiveness of combining experimental spectroscopy with computational chemistry for the structural characterization of biologically relevant ions. The findings contribute to a deeper understanding of sulfated biomolecule fragmentation and provide valuable information for future proteomic and mass spectrometric investigations.

Experimental Methods

Sample Preparation

Sulfoserine was purchased from Bachem (Bubendorf, Switzerland). Solutions were typically made to 10-3 –10-4 M, in either 70/30 or 50/50 methanol/water with 0.1 – 1% acetic or formic acid added.

Mid-Infrared Setup

In the fingerprint region IRMPD spectra were recorded on a Fourier transform ion cyclotron resonance (FTICR) mass spectrometer coupled to the beamline of the Free Electron Laser for Infrared eXperiments (FELIX), housed at a user facility on the campus of Radboud University (Nijmegen, the Netherlands). Precursor ions were transferred from the solution phase to the gas phase using a Micromass Z-spray ESI source. These ions were then trapped in the ICR cell and mass isolated using a stored waveform inverse Fourier transform (SWIFT) excitation pulse. To record IRMPD spectra of fragment ions,

photodissociation of the precursor ion was induced using a fixed-wavelength (10.6 μm) CO2 laser, and then the fragment ion of interest was mass isolated, similarly to the precursor, prior to analysis. The mass-isolated ion was then irradiated with the tunable output of FELIX (2 – 4 s, 10 Hz macropulses) and the resulting fragment ions and remaining precursor ions were mass analyzed in the ICR cell.

NH/OH-Stretching Region Setups

Two instruments were used to record the NH/OH-stretching region IRMPD spectra presented herein. The first instrument was used to record the spectrum of the precursor ion and both studied fragment ions. The second instrument was used to replicate the results for one of the fragment ions, demonstrating the robustness of the analysis method used.

The first instrument is a Thermo-Finnigan LCQ-Deca, which has been modified to include a sapphire window laser port and a hole through the ring electrode to allow passage of irradiation through the ion cloud. In this case, the irradiation source is a LaserVision OPO/A, a pulsed system. This instrument is in the laboratory of Prof. Compagnon (University of Lyon) and has thus been previously described in some detail by that group.

The second instrument is the primary experimental apparatus of the Polfer Group. Since that first report, some modifications have been made, especially to the source. This setup consists of a custom hybrid mass spectrometer coupled to a cw OPO (Linos OS4000). Briefly, it works as follows:

Ions are formed in a captive electrospray ionization source, transferred through a heated capillary for desolvation and an ion funnel for focusing, prior to being trapped in a hexapole preaccumulation trap.

After a user-defined accumulation time, the electrostatic gate trapping the ions in the hexapole is lowered and ions are transferred, via a mass selective quadrupole, to a QIT. Ions are held in the QIT for some period of time, during which fragment ions formed by CID upon transfer can be ejected and irradiation by the OPO can be performed. Ions from the QIT (typically remaining precursor ions and any resulting fragment ions) are ejected to a ToF mass analyzer. The resulting mass spectra are collected on in-house LabVIEW software (National Instruments, Austin, TX), which also facilitates the photodissociation yield analysis.

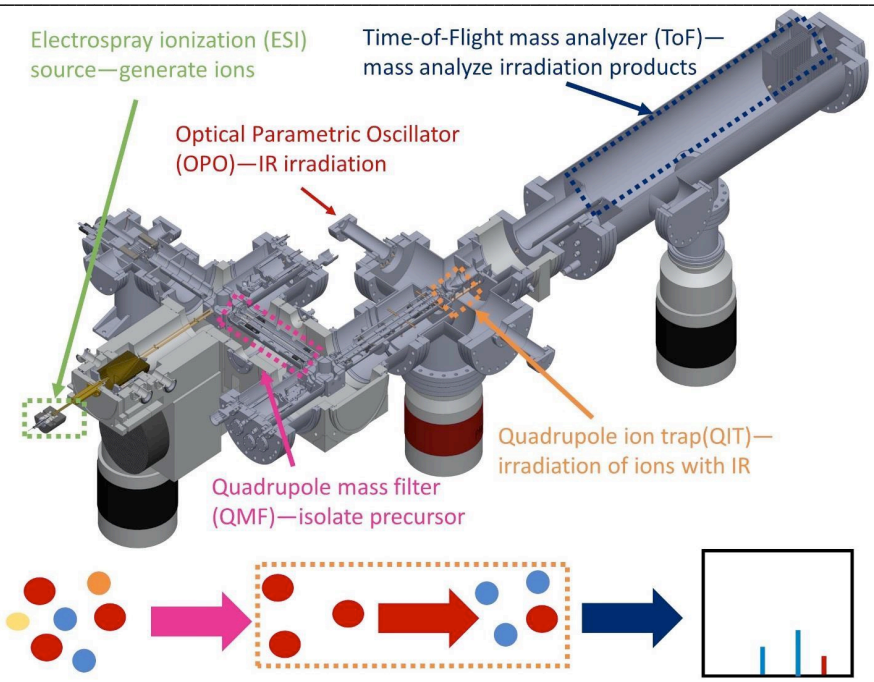

Figure 1. (Top) The Polfer Group's custom ESI-QMF-QIT-ToF mass spectrometer for IRMPD experiments. (Bottom) A pictorial overview of the IRMPD experiment on this instrument.

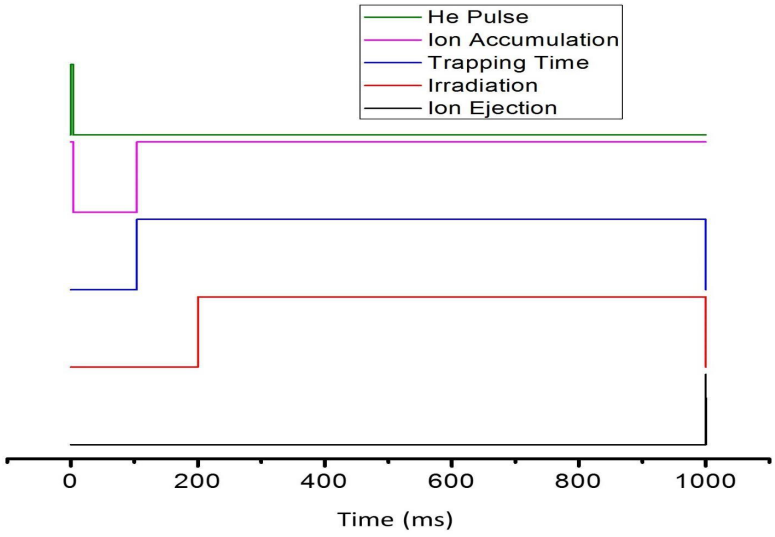

Figure 2. Example of the main timing steps involved in recording IRMPD mass spectra using the custom instrument described in Figure 1.

Figure 1 shows a representation of this instrument, with the most important ion manipulation devices highlighted and labeled. A generic timing scheme is presented in Figure 2 to give the reader an idea of how the experiment is actually accomplished.

First, helium gas is pulsed into the QIT for a short time (e.g., ~4 ms). Then ions are injected

into the QIT. This is accomplished by lowering the gate which was facilitating ion accumulation in the source hexapole to reduce ion losses in the source (since our experiment is essentially a pulsed experiment and ESI is a continuous source). Next, ions are trapped in the QIT, during which time various manipulation acts can be performed, including ramping the QIT rf to eject low mass ions. Shown in the figure, this is also the time period during which the shutter blocking the OPO (or laser) can be opened to allow for IRMPD experiments. Both trapping time and shuttering are independently controlled events of variable time length (typically ~200-2000 ms).

Finally, to complete the experiment, the results of the experiments completed in the trap are analyzed by ejecting the ions from the trap to the ToF for mass analysis.

IRMPD Yield

For all spectroscopy experiments, regardless of the instrument used for the measurement, Equation 1 was used to calculate the linear IRMPD yield, which was then plotted as a function of the wavenumber (cm-1) of irradiation to construct IRMPD spectra. For data collected with FELIX or the cw OPO, the data is linearly corrected for

fluctuations in laser/OPO power.

$$IRMPD\ Yield = \Sigma\ Iphotofragments$$

$$\Sigma\ Iphotofragments + Iprecurs \quad (1)$$

Theoretical Calculations

To aid in the structural assignment of the fragment ions, calculations were performed with the aid of Dr. Corey Stedwell. Chemical structures, including various conformations for each potential isomer, of the two fragment ions of interest were generated using Gabedit. Energy optimization and IR frequency calculations were performed using density functional theory (DFT) at the B3LYP level of theory with the aug-cc-pVTZ basis set, using the Gaussian 09 software package. Gabedit and/or Avogadro software were used for visualization of the structures, infrared spectra, and molecular motions. Scaling factors of 0.973 for the fingerprint region and 0.960 for the NH/OH-stretching region were applied, consistent with previous literature reports. Computed spectra were convoluted with a 10 cm-1 (NH/OH-stretching region) or 30 cm-1 (fingerprint region) full-width-at-half-maximum Gaussian line shape to facilitate visual comparison with experimental spectra.

Results and Discussion Collision-Induced Dissociation of Sulfoserine

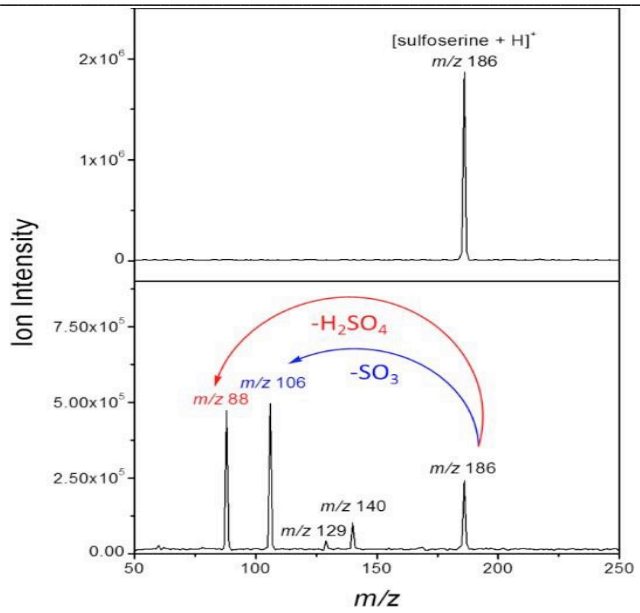

Figure 3. CID-MS of protonated sulfoserine. Reprinted from the International Journal of Mass Spectrometry, volume 379, A.L. Patrick, et al., pages 26-32, copyright 2015, with permission from Elsevier.

The collision-induced dissociation of protonated sulfoserine was measured using a normalized collision energy (NCE%) of 20 for 60 ms (see Figure 3). It was found that the two dominant fragmentation channels consist of loss of 80 Da and 98 Da, corresponding to loss of SO3 and H2SO4, respectively. While time/energy-resolved CID experiments seem to indicate that these two channels are independent, CID alone provides very few structural clues for the resulting fragment ions. A minor fragmentation channel was noted, but will not be considered further here, as it does not involve the modification.

Structural Elucidation of the m/z 106 Fragment Ion

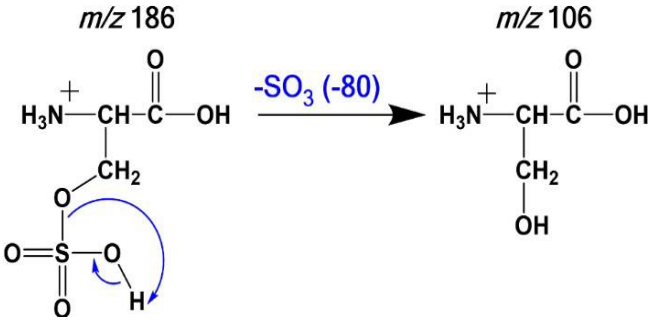

Figure 4. Hypothetical fragmentation pathway leading to the observed m/z 106 ion. Reprinted from the International Journal of Mass Spectrometry, volume 379,

A.L. Patrick, et al., pages 26-32, copyright 2015, with permission from Elsevier.

As sulfation of protonated serine causes an 80 Da increase in mass, it is likely that the loss of 80 Da from protonated sulfoserine produces a

fragment ion with a structure identical to that of protonated serine (Figure 4). This can straightforwardly be verified by comparison of an experimental IRMPD spectrum recorded for the fragment ion (m/z 106) to that obtained for commercially-available synthetic serine.

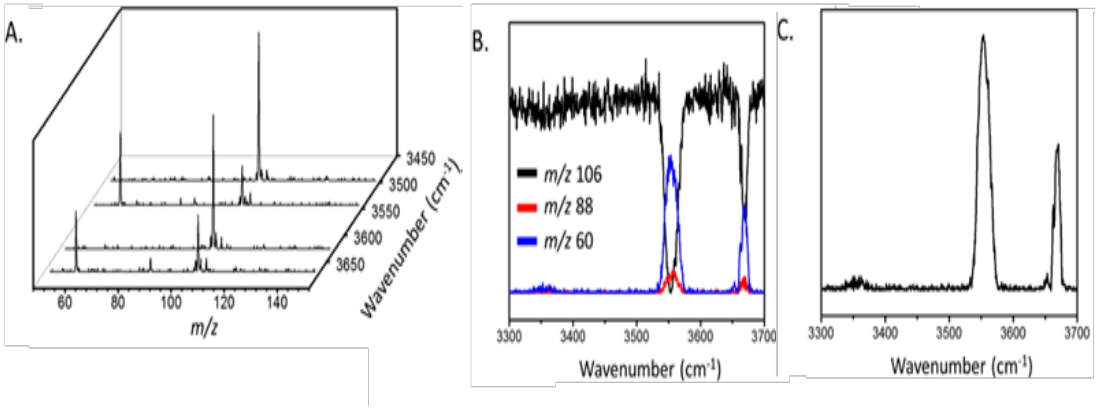

Figure 5. Steps of data acquisition and analysis: (A) recording IRMPD-MS as a function of wavenumber, (B) evaluation of integral intensities of precursor and fragment ions at each wavenumber, and (C) calculation of the IRMPD yield as a function of wavenumber

Figure 5 gives an overview of how IRMPD spectra are measured, using the m/z 106 fragment ion as an example. First, IMRPD mass spectra are recorded at discrete irradiation wavelengths for a mass-selected precursor ion (Figure 5, A).

Whereas only a few mass spectra are shown in the figure for legibility, in reality mass spectra are recorded in small wavelength steps (e.g., ~5 cm-1) across the entire range of interest. Using data processing software, the integral intensity of the precursor and fragment ions is determined for each mass spectrum. Plotting these integral intensities as a function of irradiation energy (Figure 5, B) shows that an ion-dip spectrum can be obtained from the precursor ion intensity (e.g., precursor ion intensity goes down at infrared modes) and an ion-appearance spectrum can be obtained for each of the photofragments (wherein ion intensity appears/increases at infrared absorption bands). To correct for total ion intensity fluctuations, IRMPD yield, as determined by Equation 3-1, is plotted as a function of wavenumber to generate an IRMPD spectrum (Figure 5, C). This IRMPD spectrum is what is typically used for analysis and is what is presented throughout for IRMPD spectroscopy experiments completed as part of this dissertation project.

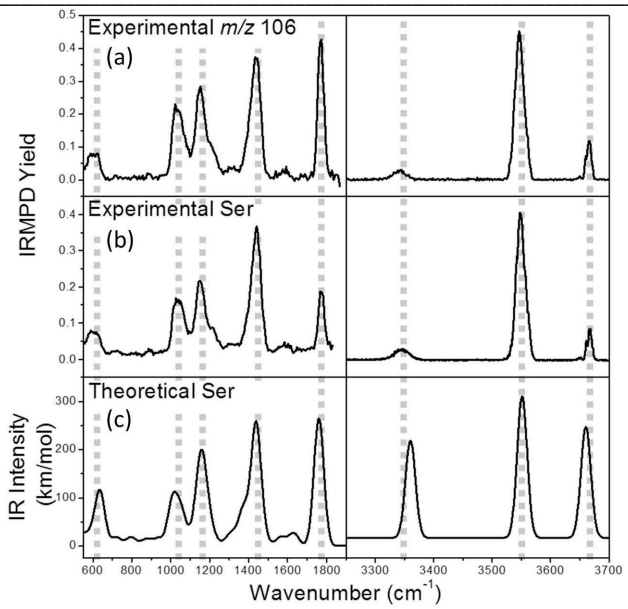

Figure 6. Experimental IRMPD spectrum of (a) the m/z 106 fragment ion and (b) protonated serine, along with (c) the theoretical IR spectrum of protonated serine. Modified from the International Journal of Mass Spectrometry, volume 379, A.L. Patrick, et al., pages 26-32, copyright 2015, with permission from Elsevier.

The spectra for the m/z 106 fragment ion and for protonated serine are provided in Figure 6 (top and middle panels). These two spectra are nearly identical. However, since a convenient synthetic standard is not always available for all proposed gas-phase ion structures, it is important to verify theoretical calculations when synthetic standards are available. Note that in Figure 6 (middle and lower panels), the match between the known synthetic standard's experimental IRMPD spectrum and the theoretical IR spectrum is very good, especially in terms of band position. It is worth noting here that it is not surprising that the predicted band intensities are not perfectly reproduced in the experimental (IRMPD) spectra. This is primarily due to the fact that the IR spectra calculated using quantum mechanical models are based on linear absorption, whereas IRMPD spectroscopy relies on a multiple photon process, with photodissociation often taking on the order of 10's of photon absorptions to occur. The good match for band positions gives confidence in this level of theory for the type of molecules of interest in this section; thus, theoretical calculations should be helpful in identifying the structure of the more interesting m/z 88 fragment ion.

Structural Elucidation of the m/z 88 Fragment Ion

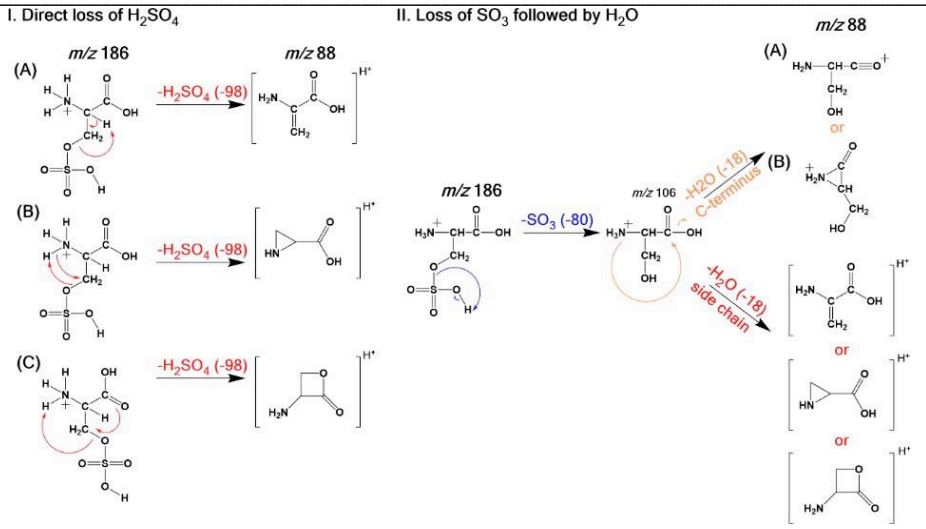

Figure 7. Potential fragmentation pathways leading to the observed m/z 88 fragment ion. Reprinted from the International Journal of Mass Spectrometry, volume 379, A.L. Patrick, et al., pages 26-32, copyright 2015, with permission from Elsevier.

The mechanism leading to the formation of the m/z 88 fragment ion—and thus the product ion structure—is less obvious. Two broad possible categories of dissociation can be considered: (1) direct loss of H2SO4 (i.e., concomitant loss pathway) or (2) loss of SO3 followed by water loss (i.e., sequential loss pathway). Such hypothetical pathways are illustrated in Figure 7.

In the first instance, the mechanism might be expected to be similar to those proposed for phosphoserine. In Figure 7, three distinct potential pathways for this instance (panel I) are given. Pathway I-A is a 1,2-cis-β-elimination of H2SO4 from the side chain, generating 2-amino-propenoic acid. Pathway I-B proceeds via a nucleophilic attack by the amino group upon the β-carbon, generating a 2-carboxy-aziridine product ion structure. Pathway I-C shows a nucleophilic attack of the carbonyl oxygen of the C-terminus upon the β-carbon to generate a product ion with a β-lactone structure. It should be noted here that the 2-carboxy-aziridine structure has been determined to be the structure present as the m/z 88 fragment ion from phosphoserine by mass spectrometric methods and IRMPD spectroscopy.

In the case of sequential losses of SO3 and H2O, the first step would be expected to generate protonated serine, as was confirmed for the observed SO3 loss in the previous section. Then, subsequent water loss could conceivably occur from the hydroxyl side-chain group or from the C-terminal carboxylic acid. Water loss from the hydroxyl side chain could form product ion structures similar to those hypothesized for the direct loss pathway. On the other hand, fragment ions formed from water loss from the C-terminus would be expected to have distinct structures. Direct loss of water from the carboxylic acid could lead to the formation of an acylium ion (II-A); however, acylium ions are generally unstable in the gas phase and would be expected to undergo spontaneous CO loss, which would shift the m/z. Alternatively, nucleophilic attack of the N-terminus on the carbonyl carbon to form a 3-membered ring could occur (II-B). However, previous literature reports indicate that side-chain water loss from protonated threonine is more favorable than C-terminal

water loss.[177] Thus, it is likely that this would also be the case for protonated serine.

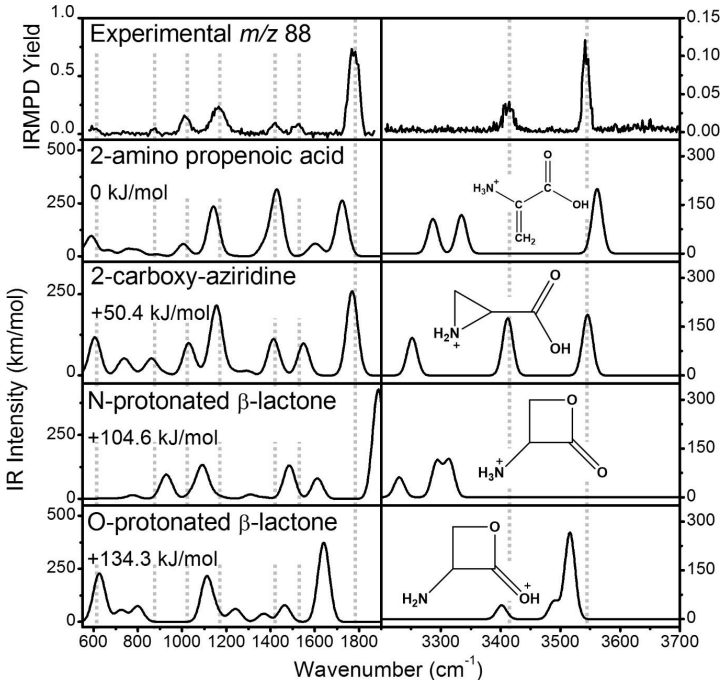

Figure 8. (Top) Experimental IRMPD spectrum of the m/z 88 fragment ion. (Lower panels) Theoretical IR spectra of the lowest energy conformers of the four candidate ion structures, with stick structures given in each panel. Reprinted from the International Journal of Mass Spectrometry, volume 379, A.L. Patrick, et al., pages 26-32, copyright 2015, with permission from Elsevier.

The experimental IRMPD spectra (both NH/OH-stretching and fingerprint regions) are given for the m/z 88 fragment ion in the top panel of Figure 8. In the hydrogen stretching region, it is notable that the carboxylic acid band (as established in the protonated serine experiment) is present. This suggests that C-terminal water loss has not occurred. Further evidence of this is given by the fact that no alcohol OH stretch is observed, suggesting that side-chain loss has indeed occurred. Taken together, these results support a side chain loss pathway.

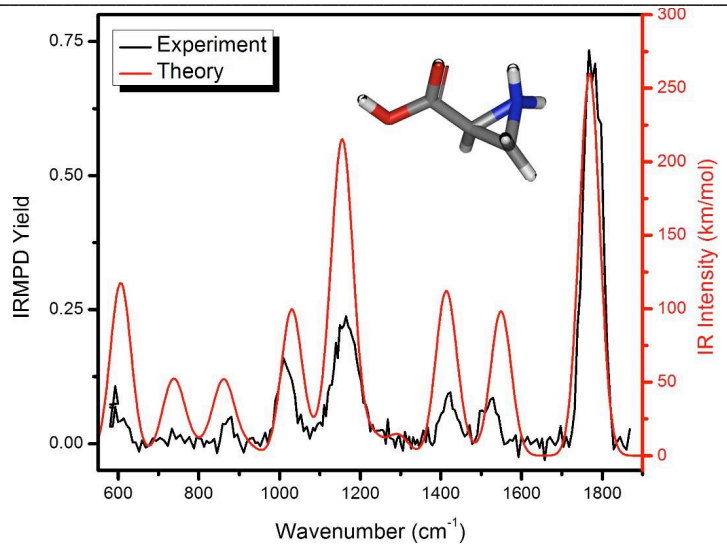

Figure 9. Direct comparison of the fingerprint IRMPD spectrum of the m/z 88 fragment ion compared to the computed IR spectrum of 2-carboxy-aziridine. Reprinted from the International Journal of Mass Spectrometry, volume 379, A.L. Patrick, et al., pages 26-32, copyright 2015, with permission from Elsevier.

To determine which side-chain loss pathway might be at play, it is necessary to compare directly to theoretical calculations. The theoretical IR spectra for the lowest- energy conformer of each fragment ion structure proposed for side-chain loss in Figure 7 are given in the lower panels of Figure 8 for comparison to the experimental IRMPD spectrum of the m/z 88 fragment ion. From this comparison, it is clear that the 2-carboxy-aziridine spectrum is the closest match. An overlay of the fingerprint region is provided in Figure 9, which illustrates this match even more convincingly. A comparison between IR bands predicted by theory and the features observed in the experimental spectrum of m/z 88 are compared in Table 1.

Table 1. Comparison of predicted bands for 2-carboxy-aziridine and experimental band s for the m/z 88 fragment ion.

Predicted Band (cm-1) B3LYP/aug-cc-PVTZ	Observed Band (cm-1) IRMPD Spectroscopy
609	600
737	--
865	873
1032	1010
1156	1159
1415	1417
1552	1529
1768	1767
3251	--
3412	3414
3545	3541

A relatively intense predicted band at 3250 cm-1 is not observed in the experimental data. There are several plausible reasons for this discrepancy. Lower-energy modes are typically more difficult to observe (see, for instance, the difference in intensity between the NH and OH stretches in the protonated serine spectrum); yet, in this case no band was observed, rather than a weak one. Hence, it is possible that anharmonicity has caused a red-shifting of the band outside of the measured region.

Such a shift would not have been predicted by the harmonic frequency calculations which were used. Furthermore, it is worth noting that this band was also missing from a similar structure reported as a fragment ion from phosphoserine.

As a side note, 2-carboxy-aziridine does not have the lowest energy of the considered isomers. Thus, it follows that the activation energy required to form the lowest-energy structure (2-amino-propenoic acid) is prohibitively high. These results underscore that gas-phase dissociation is not an equilibrium process and, thus, the thermochemistry of hypothesized product ions is often not a reliable indicator of which product ions will actually be formed. This is one reason that direct experimental probes, such as IRMPD spectroscopy, are critical to complement theory-based insights.

Inter-laboratory Reproducibility of IRMPD Spectra

Due to demanding experimental and instrumental requirements for IRMPD spectroscopy, many past experiments have relied on measurements performed relatively few times on a single instrument and/or in a single lab. This brings up some questions, especially in the light of some instances in which ion conformers/protonation isomers can change based on a given instrument and/or experimental parameters. In the present experiment, the m/z 88 ion was measured on two distinct experimental apparatus, with some key differences, such as the OPO (pulsed versus cw) and the mass analyzer (QIT versus ToF) used. These results are compared in Figure 10. It is notable that the two spectra are qualitatively (e.g., band positions and peak shapes) very similar—demonstrating the robustness and reliability of these measurements.

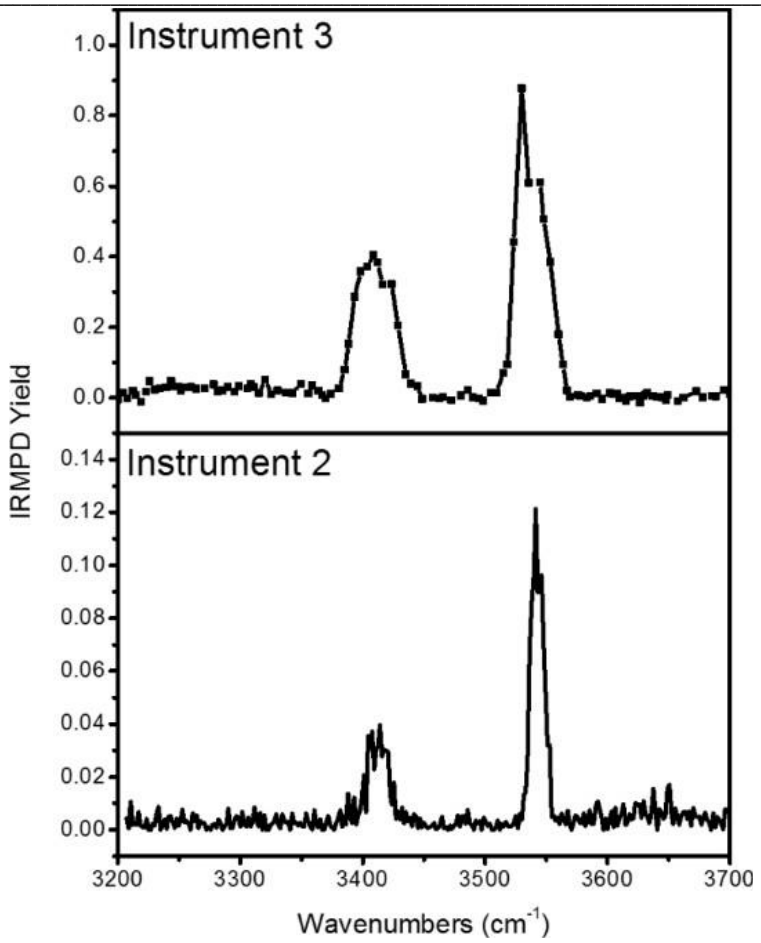

Figure 10. Inter-setup reproducibility of the IRMPD spectrum of the m/z 88 fragment ion in the NH/OH-stretching region. Data recorded on the Polfer group's hybrid instrument (Instrument 3) and the Thermo LCQ described in this chapter (Instrument 2). Reprinted from the International Journal of Mass Spectrometry, volume 379, A.L. Patrick, et al., pages 26-32, copyright 2015, with permission from Elsevier.

The main difference between the spectra are the absolute magnitude of the peaks. Given the efficient photofragmentation produced by the same model pulsed OPO when coupled to the Polfer Group's hybrid instrument, this discrepancy in fragmentation yield is likely mostly due to trapping conditions during irradiation. Specifically, the LCQ is operated at a static pressure; whereas, the QIT on the Polfer Group instrument has a pulsed trapping gas, which is pumped away prior to irradiation. It has previously been shown that lower pressures improve IRMPD yield because the competition from collisional cooling is reduced and ions are more likely to overcome their dissociation thresholds on a timescale compatible with the IRMPD process. If the OPO does contribute to the difference, it may be due to inconsistencies in, for instance, beam focusing and ion cloud overlap between the two setups.

Conclusion

The experiments presented herein represent the first direct structural analysis of the fragmentation pathways of sulfoserine using ion spectroscopy. CID of protonated sulfoserine abundantly produces two fragment

ions arising from modification (i.e., SO3 and H2SO4) loss. SO3 loss generates a fragment ion identical to protonated (unmodified) serine, as confirmed by comparisons to experiment and theory. H2SO4 loss generates, in a kinetically-controlled fragmentation process, an m/z 88 ion adopting a 2-carboxy-aziridine structure. When compared to previous results for phosphoserine,[158] it appears that sulfoserine has more competing fragmentation pathways than phosphoserine, but that for the m/z 88 ion—which is observed for both precursor ions—a similar structure is obtained regardless of precursor, suggesting a similar fragmentation pathway. A key area for future experiments is to examine larger systems, where additional differences between sulfated and phosphorylated systems may be found. Recently, a theoretical and experimental study on the fragmentation behavior of sulfopeptides was published by another group.

References

1. Patrick, A. L., Stedwell, C. N., Polfer, N. C. Structural elucidation of sulfoserine fragment ions by IRMPD spectroscopy. International Journal of Mass Spectrometry. 2015;379:26–32.
2. Polfer, N. C., Oomens, J. Vibrational spectroscopy of bare and solvated ionic complexes of biological relevance. Mass Spectrometry Reviews. 2009;28(3):468–494.
3. Oomens, J., Sartakov, B. G., Meijer, G., von Helden, G. Gas-phase infrared multiple photon dissociation spectroscopy of mass-selected molecular ions. International Journal of Mass Spectrometry. 2006;254:1–19.
4. Stedwell, C. N., Patrick, A. L., Polfer, N. C. Infrared ion spectroscopy for structural characterization of biomolecular ions. Analytical Methods. 2013;5:1806–1816.
5. Zhang, X., Julian, R. R. Investigation of peptide fragmentation pathways using tandem mass spectrometry. Journal of the American Society for Mass Spectrometry. 2011;22:1238–1245.
6. Paizs, B., Suhai, S. Fragmentation pathways of protonated peptides. Mass Spectrometry Reviews. 2005;24:508–548.
7. Harrison, A. G. Peptide and protein fragmentation under collision-induced dissociation conditions. Mass Spectrometry Reviews. 1997;16:201–217.
8. Tureček, F. Nucleophilic substitution and rearrangement reactions in peptide ion fragmentation. Journal of Mass Spectrometry. 2003;38:1–14.
9. O'Hair, R. A. J. The role of nucleophilic processes in peptide fragmentation. Mass Spectrometry Reviews. 2000;19:274–297.
10. Aebersold, R., Mann, M. Mass spectrometry-based proteomics. Nature. 2003;422:198–207.
11. Jensen, O. N. Modification-specific proteomics. Current Opinion in Chemical Biology. 2004;8:33–41.
12. Seibert, C., Sakmar, T. P. Toward a framework for sulfoproteomics. Molecular BioSystems. 2008;4:104–111.
13. Medzihradszky, K. F. Characterization of protein post-translational modifications by mass spectrometry. Nature Methods. 2005;2:593–602.
14. Gaussian 09 User Reference Manual. Gaussian Inc., Wallingford, CT, USA; 2009.
15. Frisch, M. J., Trucks, G. W., Schlegel, H. B., et al. Gaussian 09, Revision D.01. Gaussian Inc.; 2009.
16. Becke, A. D. Density-functional thermochemistry III: The role of exact exchange. Journal of Chemical Physics. 1993;98:5648–5652.
17. Lee, C., Yang, W., Parr, R. G. Development of the Colle–Salvetti correlation-energy formula into a

functional of electron density. Physical Review B. 1988;37:785–789.
18. Ditchfield, R., Hehre, W. J., Pople, J. A. Self-consistent molecular orbital methods. Journal of Chemical Physics. 1971;54:724–728.
19. Oomens, J., Steill, J. D. Free-electron laser spectroscopy of isolated biomolecular ions. Journal of Physical Chemistry A. 2008;112:3281–3283.
20. Polfer, N. C. Infrared spectroscopy of trapped molecular ions. Chemical Society Reviews. 2011;40:2211–2221.